Adsorption (2024) 30:1193–1203
https://doi.org/10.1007/s10450-024-00493-4

Improving the adsorption capacity of graphene oxide. Effect of Ca^{2+} on tetracycline retention

Florencia M. Onaga Medina[1] · Marcelo J. Avena[2] · María E. Parolo[1]

Received: 19 May 2023 / Revised: 9 May 2024 / Accepted: 9 May 2024 / Published online: 25 May 2024

Abstract

Tetracyclines (TCs) constitute a group of antibiotics that are commonly used to treat bacterial diseases, in veterinary medicine and as an additive in animal feed. This broad application has led to their accumulation in food products and the environment because sewage treatment plants cannot completely remove them. Therefore, the aim of this study was to synthesize graphene oxide (GO) and evaluate its TC adsorption properties in aqueous media. The effects of pH (between 2.5 and 11) and Ca^{2+} concentration (between 0 and 1 M) were thoroughly investigated. Structural, textural, and electrokinetic properties of the prepared GO were determined by N_2 adsorption/desorption, XRD, TEM, UV–vis, FTIR, XPS, thermogravimetry and electrophoretic mobility measurements. TC adsorption on GO is an interplay between the two main roles played by Ca^{2+}: competitor or bridging cation. At low pH, there is cation exchange, and Ca^{2+} behaves as a competitor of the positively charged TC species, decreasing adsorption as calcium concentration increases. At high, the formation of Ca bridges between the surface and TC (GO-Ca^{2+}-TC) is favored, increasing the adsorption of the antibiotic by increasing calcium concentration. Different combinations of Ca^{2+} and pH effects are important to improve the use of GO either as a pH-dependent and reversible TC adsorbent for decontamination or as pH-independent adsorbent for TC quantification with electrochemical sensors.

Keywords Tetracycline · Adsorption · Graphene oxide · Calcium effect · Nanoadsorbents

1 Introduction

Tetracyclines (TCs) constitute a group of antibiotics, some natural and others obtained by semi-synthesis, that cover a wide spectrum of antimicrobial activity. In addition to urinary tract infections, chlamydia, and acne, TCs can also be used to treat other bacterial infections such as respiratory tract infections, skin, soft tissue infections, among others [7, 24, 41, 50]. The wide use of these antibiotics in veterinary medicine and also as an additive in animal feed, have brought as a consequence its presence in food products such as meat, milk, honey and chicken [10, 13, 48]. TCs is not limited to food; they can also enter the environment because sewage treatment plants cannot completely remove them [26]. Moreover, there is a growing environmental concern about antibiotics because their presence in soils and waters leads to the emergence of resistant species. High concentrations of TCs and three degradation products were reported in the effluents (5.28–8.32 μg L^{-1}) and sludges (34.6–49.6 μg kg^{-1}) of three municipal wastewater treatment plants located in Turkey [64] and in aquatic organisms (4.23 to 208.14 ng g^{-1}) [20]. Given these concerns, the development of analytical methodologies that allow the determination of low concentrations of tetracycline in environmental matrices is crucial. Among the analytical methods reported in different works, HPLC, ELISA, capillary electrophoresis, spectrophotometry, chemiluminescence and electrochemical approaches stand out [1, 9, 40, 42, 48, 56, 68]. The main disadvantages of these techniques are that they have tedious sample pretreatment processes and long analysis times [33]. On the other hand, electrochemical sensors are an attractive alternative for the detection of TCs due to their high selectivity, rapid detection and possibility of in situ applications [33]. Graphene materials, as constituent

✉ María E. Parolo
maria.parolo@fain.uncoma.edu.ar

[1] Centro de Investigaciones en Toxicología Ambiental y Agrobiotecnología del Comahue (CITAAC), Facultad de Ingeniería, CONICET-Universidad Nacional del Comahue, Buenos Aires 1400, 8300 Neuquén, Argentina

[2] Instituto de Química del Sur (INQUISUR), Departamento de Química, CONICET-Universidad Nacional del Sur. Av. Alem 1253, 8000 Bahia Blanca, Argentina

of electrochemical sensors, seem to have adequate properties for these applications. Nanomaterials composed of graphene oxide (GO) have high surface area and high specific capacitance due to its unique structure, which allows it to store a large amount of electrical charge. In addition, GO has oxygenated functional groups, such as epoxide (C–O–C), hydroxyl (C–OH), and carboxyl (-COOH) groups, which are located both in the basal planes and at the edges of the material [8, 54]. These characteristics make them appropriate for the adsorption of different classes of compounds and therefore, for applications such as electrochemical sensors and biosensors for the determination, for example, pesticides, drugs, nitrogenous bases and others [16, 18, 35, 64, 67, 71]. Wong et al. [66] fabricated a carbon paste electrode by combining multiwalled carbon nanotubes and graphene oxide for TC detection. They applied adsorption separation differential pulse voltammetry (AdSDPV) in which tetracycline was firstly electro accumulated and then analyzed. This technique only detects those analytes that are strongly adsorbed on the electrode surface. The sensor was applied to different samples such as artificial urine, river water and pharmaceutical samples. Lorenzetti et al. [34], on the other hand, applied a modification of AdSDPV to determine TC in milk and river samples using disposable screen-printed electrodes. The technique allowed analysts to improve the selectivity of electrochemical sensors by exploiting the adsorption properties of the sensing surface [43].

Within the tetracycline's family, the so-called tetracycline (TC) is one of the substances that constitute this group of antibiotics. It has different acid groups in its structure and can exist under different ionic species and conformations depending on the pH. The presence of such groups in the TC molecule generates potential sites of interaction with metal ions and surfaces [46].

The adsorption of TC on montmorillonite, mesoporous silice, graphene-based materials and others adsorbents have been previously studied [6, 17, 19, 39, 45, 52]. Nevertheless, there is very little information on the TC adsorption in the presence of a divalent cation such as Ca^{2+} under different pH conditions. This cation is ubiquitous in natural media and is implicated in many biological and environmental processes. There are studies regarding its influence on the adsorption of different organic and inorganic compounds on different adsorbents [4, 28, 29, 31, 32, 59]. Chowdhury et al., [11] studied the influence of pH, ionic strength, ion valence and the presence of natural organic matter (NOM) on the aggregation and stability of graphene oxide (GO) and three reduced GOs (rGO). They found that the stability depended on pH, ion valence, and concentration of surface functional groups. In the presence of divalent cations (Ca^{2+}, Mg^{2+}), the increase in pH decreased the stability of GO, which was due to Ca^{2+} adsorption on the surface functional groups of GO. In the presence of NOM and divalent cations (Ca^{2+}, Mg^{2+}), GO aggregates settled from suspension because Ca^{2+} ions act as bridges between GO functional group and NOM. This indicates that pH and divalent cations can play complex roles in the adsorption properties of rGO and GO and could affect significantly adsorption and detection of third molecules such as tetracyclines.

The present work focuses on obtaining GO nanoparticles with TC adsorption properties for a future application as electrochemical sensors or as TC sorbents for decontamination. The synthesis and structural characterization of GO is firstly presented, followed by an evaluation of the TC adsorption properties. Special attention is paid to the effects of Ca^{2+} on the adsorption at different pH, which could be used to optimize the performance of GO as a sensor or as a TC adsorbent.

2 Materials and methods

2.1 Materials

Graphite powder (Gr) with a particle size < 50 µm was supplied by Sigma-Aldrich. $KMnO_4$ (99.5%), H_2SO_4 (95–98%), H_3PO_4 (85%) and HCl (36–38%) were supplied by Cicarelli. Hydrogen peroxide (30% v/v) was supplied by Anedra and ethanol (96%) was supplied by Porta. Tetracycline hydrochloride (TC, purity 99%) was obtained from Parafarm and was used without further purification. TC stock solutions were prepared just before use to avoid degradation caused by oxygen and light. $CaCl_2$ and 0.01 M KCl solutions were used for Ca^{2+} effect experiments and as electrolyte for zeta potential measurements. NaOH and HCl solutions were used for pH adjustment.

2.2 Synthesis of graphene oxide

GO was synthesized using Tours' method [37]. A 9:1 mixture of H_2SO_4:H_3PO_4 (360:40 mL) was added to Gr powder (3.0 g) and $KMnO_4$ (18.0 g), producing a slightly exothermic reaction, which increased the temperature of the reaction vessel to 35–40 °C. The product of the reaction was then heated to 50 °C and stirred for 12 h, cooled at room temperature and poured afterwards onto ice (~ 400 mL) with 30% H_2O_2 (3 mL). This last procedure produced important bubbling, a yellow coloration on the product, which finally became brownish. The resulting mixture was centrifuged (10,000 rpm for 20 min), and the supernatant was discarded. The remaining solid material was washed first with 200 mL water, then with 200 mL 30% HCl, and finally with two washings of 200 mL ethanol. The washed material was dried overnight at 42 ºC in air. The obtained brown material will be referred as GO hereafter.

2.3 Characterization techniques

Textural characterization of Gr and GO were conducted with N_2 adsorption/desorption isotherms at 77 K using a Micromeritic Gemini V2.0 2380 equipment. Samples were degassed at 323 K for approximately 12 h. Surface area values were calculated from the linear adjustment of the Brunauer–Emmett–Teller (BET) equation with adsorption data obtained in the relative pressure (p/p◦) range between 0.01 and 0.33. The total pore volume and the average pore size were obtained by the Barrett-Joyner-Halenda (BJH) method. X-ray diffraction (XRD) patterns were obtained with a Rigaku D-Max II-C diffractometer, with CuKα radiation (λ = 1.54 Å) of 40 kV and 20 mA. Scans were recorded between 5 and 60° 2θ, with a step size of 0.02° 2θ and a scanning rate of 2° min^{-1}. Crystal dimensions were calculated using the Scherrer equation. The morphology of GO was characterized using transmission electron microscope (TEM, JEOL 100 CX) images. The TEM micrographs of the GO sample were collected at a maximum accelerating voltage of 100 kV. The sample was prepared by dispersing a small amount of GO in ethanol via sonication for about 15 min. A few drops of this suspension were placed in 200 mesh grids provided with a Formvar film. FT-IR spectra were obtained with a IRTracer-100 Shimadzu spectrophotometer. The sample was prepared in KBr pellets with 0.3% w/w of GO or Gr. The spectra were recorded between 400 and 4000 cm^{-1} with a 4 cm^{-1} resolution and a 32 min^{-1} acquisition rate. X-ray Photoelectron Spectra (XPS) were obtained with a Thermo Scientific K-Alpha + X-ray Photoelectron Spectrometer. Spectra were recorded at room temperature, using Al-K (1200W) radiation for excitation and a 180° double focus hemispherical analyzer in a vacuum chamber of 1–10 mbar. Spectra were collected for oxygen (O1s), carbon (C1s) and a survey to identify the different species. The deconvolution of the spectra was obtained by means of Igor software using Voigt functions. Thermogravimetric analyses (TGA) data were recorded on a Mettler Toledo TGA/DSC1 instrument, the samples were heated from room temperature to 1000 ºC (10 ºC min^{-1}) in N_2 atmosphere. UV–Vis spectra were collected in the range of 200–700 nm using a Genesis 10S UV–Vis Spectrophotometer (Thermo Scentific). A zetasizer (Nano-ZS) Malvern equipment was used to determine the zeta potential of Gr and GO particles at different pH values. Gr and GO suspensions were prepared in 0.01 M KCl solutions, the pH was adjusted to the desired value and after 15 min equilibration, the electrophoretic mobility was measured. Zeta potential was calculated using the Smoluchowski equation. The effects of Ca^{2+} on the electrophoretic mobility of GO at different pH values were also evaluated. For this, a stable GO dispersion was prepared in 0.01 M KCl as electrolyte and in presence of different $CaCl_2$ concentration (0.001 M and 0.01 M). The pH was modified gradually in all cases, and after equilibration the mobility was measured.

2.4 Adsorption studies

Adsorption studies under equilibrium conditions were carried out to investigate the removal capacity of tetracycline (TC) and the effects of pH and Ca^{2+} on it. Batch adsorption experiments were carried out in 10 mL glass flasks continuously shaken with an orbital shaker (200 rpm) at 22 ± 1 °C in duplicate. The concentration of TC in the equilibrium solution was quantified by UV–Vis spectrophotometry. Since the wavelength of the absorption maximum of TC changes with pH and presence of Ca^{2+}, calibration curves in the concentration range of 0–48 mg L^{-1} were performed at the corresponding pH values, with and without 0.01 M $CaCl_2$.

The equilibrium adsorption capacity (Q_e, mg g^{-1}) of GO was calculated as

$$Q_e = \frac{(c_i - c_e)V}{m}$$

where c_i and c_e are the initial and equilibrium TC concentrations, V is the volume and m the mass of adsorbent used in the experiments. The ratio m/V is known as the adsorbent dose.

To acquire optimal adsorption experimental condition, the effects of some operation parameters (i.e., adsorbent dose, TC initial concentration and pH solution) on TC adsorption were explored. The effect of adsorbent mass was evaluated at an initial concentration of 30 mg L^{-1} and pH 5.

Adsorption isotherms at 22 °C were performed in 10 mL capped glass vessels varying TC initial concentration from 20 to 90 mg L^{-1} with the same adsorbent dose (250 mg L^{-1}). Two pH values were investigated (5 and 9.5). Once equilibrated, the dispersions were filtered with 0.45 µm filter, and the supernatant separated for TC quantification. Similar adsorption experiments were performed in the presence of 0.01 M Ca^{2+}, in order to evaluate the effects of calcium in the adsorption behavior of GO.

The effect of pH on TC adsorption was investigated in the pH range 2.5–11.0. The initial concentration of TC was 30 mg L^{-1}, and the adsorbent dose was 250 mg L^{-1}. Capped glass vessels with a total volume of 10 mL were used. The pH effect was also analyzed in the presence of 10^{-2} and 10^{-3} M Ca^{2+}.

Additional experiments to evaluate the effect of Ca^{2+} on TC adsorption were performed at constant pH and varying calcium concentration. The initial concentration of TC was 30 mg L^{-1}, the adsorbent dose was 250 mg L^{-1} and the final volume was 10 mL. Used Ca^{2+} concentrations were

0.0001 M, 0.001 M, 0.01 M, 0.1 M and 1.0 M, at two different pH values, 2.5 and 9.5.

For the adsorption – desorption cycle test, 62.5 mg of the adsorbent was added into a 250 mL TC solution (30 mg/L) in absence (pH 5) and presence of Ca^{2+} (0.01 M) at pH 9 for 24 h. The first adsorption capacity was calculated as previously described. The adsorbent with tetracycline-adsorbed was regenerated by immersing it into water at pH 5 and water containing 0.01 M Ca^{2+} at pH 9. Then, the adsorbent was reused in adsorption experiments. The removal efficiency was obtained on the basis of the initial adsorption capacity. The extra adsorption – desorption processes were repeated four times.

3 Results and discussion

3.1 Characterization

The results obtained by N_2 adsorption/desorption experiments are listed in Table S1, in the Supporting Information. Gr has a BET area of 14 $m^2\ g^{-1}$, which increased to 30 $m^2\ g^{-1}$ after the oxidation process. The average pore size of GO is 5.6 nm, indicating that it is a mesoporous material. In comparison with others graphene oxide obtained from natural graphite and oxidized by a modified Hummers method [28, 29], the studied sample has intermediate specific surface area and pore volume [5, 28, 29, 58, 61]. The pH values of Gr and GO dispersions (Table S1, in the Supporting Information) also indicate that GO exhibits strong acidity while Gr is almost neutral (slightly acidic).

The XRD patterns and structural parameters of Gr and GO are shown in Fig. 1A and B, and listed in Table S2 in the Supporting Information, respectively. Gr shows three main reflections around 26.6°, 44.7°, and 54.8° 2θ corresponding to (002), (101), and (004) crystallographic planes, respectively. The intense and sharp peak of the (002) plane suggests a highly ordered material, with multiple graphene layers [38]. After the oxidation, the peak at 26.6° 2θ disappeared as a consequence of the complete oxidation of Gr [21] and a typical peak associated to GO ((001) plane) appeared at around 9.26º 2θ. These findings are indicative of a significant reduction of the close-packed hexagonal structure and an increase of stacking disorder due to the existence of intercalated oxygenous groups [70]. The increase in the interlayer spacing (from 0.34 nm to 0.95 nm) was attributed to the conversion of sp^2 carbon to sp^3 carbon, evidencing GO oxidation and exfoliation [53, 62].

The crystallites height (Lc) decreased after oxidation from 21.49 nm in Gr to 12.06 nm in GO (Table S2, in the Supporting Information). The layer separation in graphene oxide enhanced by oxygenated functionalities is also evidenced by TEM analysis (Fig. 1C). Dark areas indicate the thick stacking nanostructure of several graphene oxide sheets. More transparent areas indicate thinner films of a few layers of GO resulting from exfoliation [60]. As it was reported in the literature, the wrinkled morphology is attributed to the presence of a large number of functional groups such as hydroxyl and carboxyl groups on the edge, and carboxyl and epoxide groups in the inner part of GO [12].

The FT-IR spectra of Gr and GO, displayed in Fig. 2A and B, show characteristic vibration bands of these materials. Gr

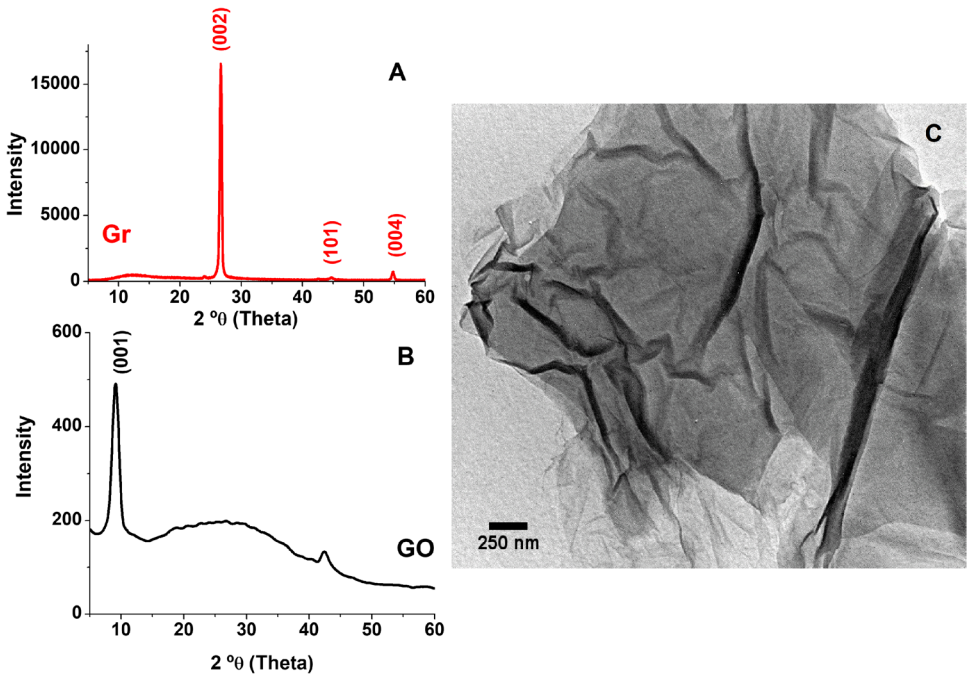

Fig. 1 (**A**) XRD pattern of Gr. (**B**) XRD pattern of GO. (**C**) TEM micrograph of GO

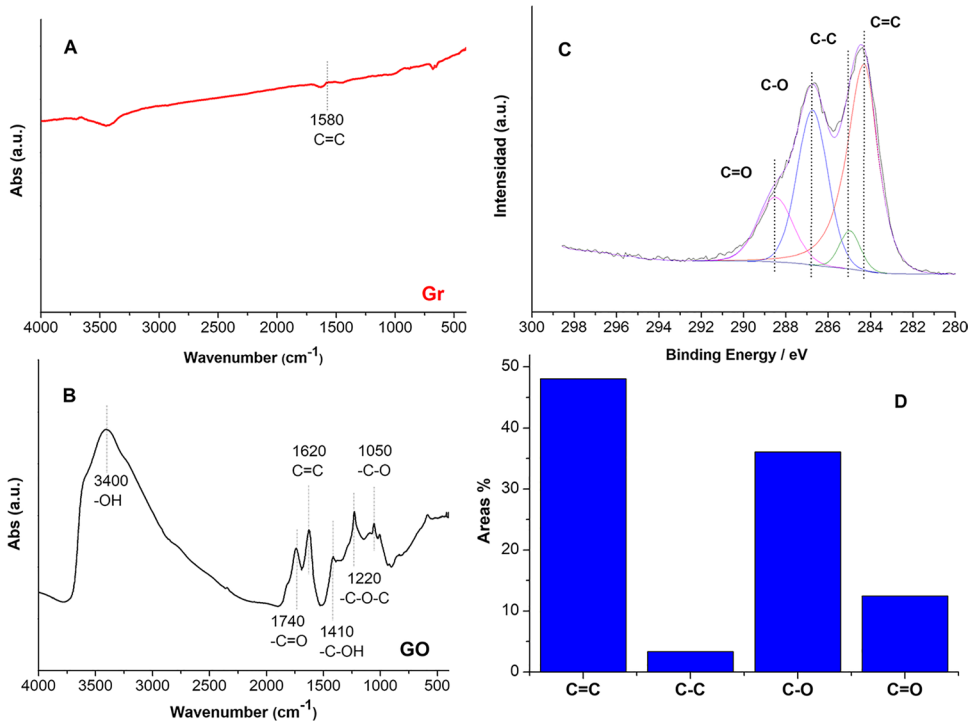

Fig. 2 (**A**) FTIR spectra of Gr in KBr pellets. (**B**) FTIR spectra of GO in KBr pellets. (**C**) XPS spectrum of GO. (**D**) Relative proportions of C1s signals of GO

spectrum resulted to be relatively flat, with weak signals. The band at 1580 cm^{-1} is attributed to the C = C vibration of graphene sheets. The spectrum of GO was very different, with stronger signals. The most intense band appears at 3400 cm^{-1} and corresponds to the O–H stretching vibration of hydroxyl groups and water molecules. The deformation vibration mode of O–H groups appears at around 1410 cm^{-1}. The band at 1740 cm^{-1} was associated to the C = O stretching vibration of a carbonyl group; another band at approximately 1620 cm^{-1} was attributed to the C = C skeletal vibration of the graphene sheets (unoxidized graphitic domains) [55]; a band appearing at 1220 cm^{-1} was in turn attributed to the stretching vibration of epoxy C–O–C group; and the band at 1050 cm^{-1} was finally assigned to the alkoxy C-O stretching vibration (carboxyl group) [2, 15, 65]. A comparison of Gr and GO spectra clearly indicates that GO is the material with the highest proportion of oxygenated groups.

The presence of oxygenated groups on GO was also detected by XPS. The elemental analysis obtained by XPS indicated C: 64.3 atom%, O: 32.1 atom%, N: 1.9 atom% and S: 1.6 atom%. The C/O ratio equal to 2 indicates a successful introduction of oxygen atoms into the ordered arrangement of graphite structure. The C1s XPS signal shows different types of carbon components. The C1s spectrum show four peaks that correspond to the following functional groups: carbon sp2 (C = C, 284.2 eV), carbon sp3 (C–C, 284.9 eV), epoxy/hydroxyls (C-O, 286.8 eV), and carbonyl (C = O, 288.6 eV) (Fig. 2C) [49, 69]. The relative proportion of these groups is shown in Fig. 2D.

Figure 3A shows the TGA of Gr and GO and Fig. 3B shows the DSC of GO, all performed in N_2 atmosphere. Gr was stable in the whole range of temperature analyzed. On the contrary, GO begun to decompose at approximately 50ºC, and lost up to 85% of its total weight when heated to 200ºC. The first endothermic peak is due to water desorption, with around 10% of mass loss. The higher mass loss occurred between 150–190 °C, with two marked exothermic peaks at 162 and 181 °C. This high thermal reactivity of GO can be attributed to the decomposition of the labile oxygen-containing moieties, promoted by the disruption of the multilayered stacks structure of GO [16, 18, 23].

The UV–vis spectrum of GO is shown in Fig. S1, in the Supporting Information. It presented a characteristic absorption band at 230 nm and a broad shoulder at 300 nm, which can be assigned to the π-π* transition of the C = C bonds and n-π* transition of the C = O bonds (carbonyl or carboxyl group), respectively. The presence of the shoulder at 300 nm is a good evidence of oxidation [25, 27, 47]. On the contrary, Gr particles settled so quickly that only a clear supernatant remained, and that is what is observed in the UV–visible absorption spectrum.

The electrokinetic properties of Gr and GO are shown in Fig. 4A. Gr had a negative zeta potential of around -22 mV at high and intermediate pH, and then the potential decreased as the pH decreased, reaching a nearly isoelectric point at pH 2.1. GO, on the contrary, exhibited a more negative zeta potential in the whole range of pH

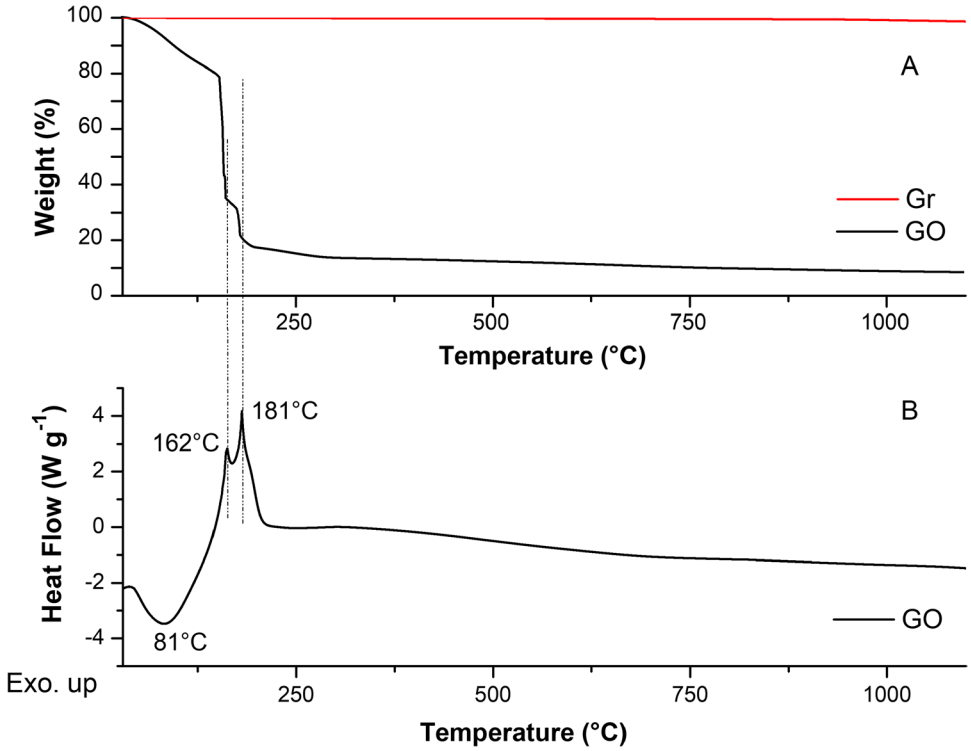

Fig. 3 (**A**) TGA analysis corresponding to Gr and GO under N_2 atmosphere. (**B**) DSC plot of GO

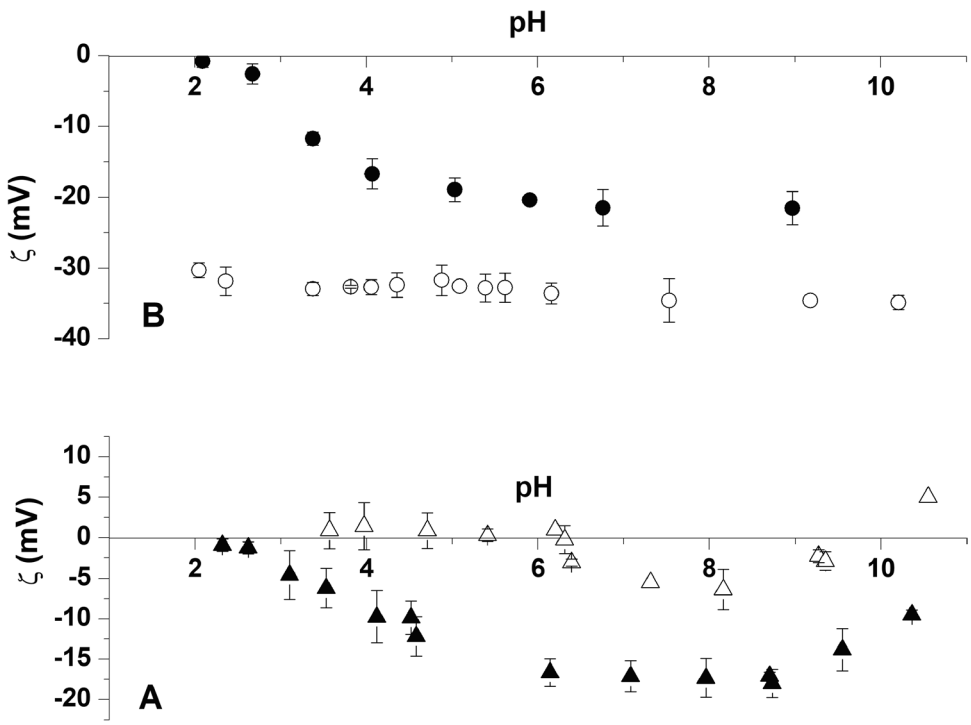

Fig. 4 (**A**) Zeta potential (ζ) as a function of pH in 0.01 M KCl: Gr (●) and GO (○). (**B**) Zeta potential (ζ) of GO in the presence of $CaCl_2$: GO with $CaCl_2$ 10^{-2} M (Δ) and GO with $CaCl_2$ 10^{-3} M (▲)

investigated. It only decreased from -35 mV to -30 mV from pH 10.5 to pH 2.1. The negative zeta potential is in line with the fact that oxidation treatment introduced oxygen-containing functional groups on the surfaces of GO [28–30, 57]. Consequently, GO suspensions resist more aggregation and tend to disperse better than Gr. Figure 4B shows that calcium produces significant changes to the electrokinetic behavior of GO. The zeta potential becomes less negative as calcium concentration increases, and the isoelectric point shifts to pH around 6 in 10^{-2} M calcium, evidencing interaction of Ca^{2+} with the surface groups of GO.

3.2 Adsorption studies

Figure S2 exhibits that TC removal capacity (%) on GO increases with the adsorbent dose from 50 to 500 mg L^{-1} at pH 5. A dose of 250 mg L^{-1} was selected to study the effect of concentration, pH and Ca on the adsorption of TC on GO. A dose of 250 mg L^{-1} results in a removal of 60%, which allows the effect of the experimental variables on the adsorption of CT to be analyzed.

TC adsorption isotherms on GO at pH 5 and 9 are presented with Langmuir settings in Fig. 5 and Table 1. TC adsorption decreased with increasing pH from 5 to 9.5 in absence of $CaCl_2$. In the literature, the pH was found to impact similarly the adsorption of TC on different solids [36, 44],Topal and Arslan, 2020). The results suggest that electrostatics interactions are playing a role on the adsorption, because the adsorbent is negatively charged in the analyzed pH range (Fig. 4A) and TC species increase their negative charge as pH increases [44]. In fact, at pH 5 TC is present in the zwitterionic ($TCH^{\pm}$) and anionic (TCH^{-}) forms, whereas at pH 9.5 it is in its negative and doubly negative forms (TCH^{-} and TC^{2-}). Even though the net charge of $TCH^{\pm}$ and TCH^{-} is 0 and -1, respectively, both species contain a positively charged group in their structure, the dimethylammonium group and thus, the molecules can arrange at the surface locating the positively charged group close to the surface and the negatively charged group(s) as far as possible from the surface [45], resulting in adsorption at pH 5. At pH 9.5, repulsive forces seem to prevail, and adsorption is nearly zero. These results were also corroborated by the pH effect adsorption assay (see below).

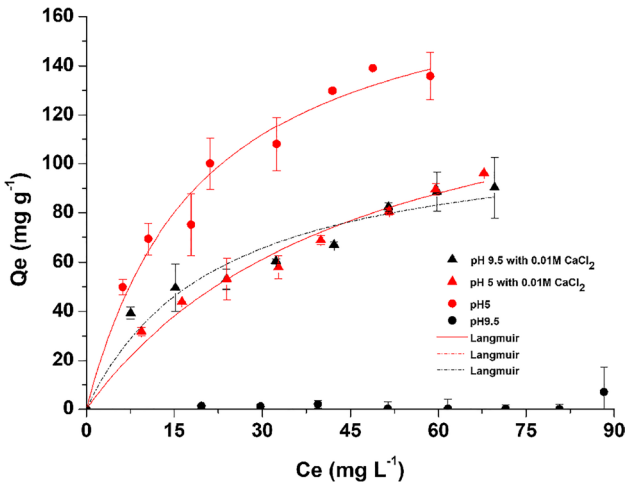

Fig. 5 Adsorption isotherms and Langmuir settings of TC on GO: at pH 5 with 0.01 M $CaCl_2$ (▲) and without 0.01 M $CaCl_2$ (●); at pH 9.5 with 0.01 M $CaCl_2$ (▲) and without 0.01 M $CaCl_2$(●)

The effect of Ca^{2+} on TC adsorption isotherms at pH 5 and 9.5 is also shown in Fig. 5. The isotherms practically did not change by changing the pH in the presence of calcium. At pH 5 the presence of calcium decreased the removal capacity of GO, whereas at pH 9.5 the divalent cation significantly increased the removal capacity. The result was that isotherms practically coincided at pH 5 and 9.5, when calcium was present. It is possible that at pH 5 Ca^{2+} competes with the positively charged group of TC species, decreasing the adsorption. This competition is no longer operative at pH 9.5, where an opposite Ca^{2+} effect was observed, probably as a consequence of the interaction of the divalent cation with negatively charged groups of the GO surface and negatively charge groups of TC species. Parolo et al., [46] reported the same effects of calcium on TC adsorption on the negatively charged montmorillonite surface, postulating the formation of Ca^{2+} bridges between the surface and TC. This seems to be also the case with GO, with Ca^{2+} forming GO-Ca^{2+}-TC bridges and thus inducing the adsorption of negatively charged TC species on a negatively charged surface.

As it is shown in Table 1, the TC adsorption capacity of GO is comparable to other graphenic adsorbents reported in the literature. There are results informed for pure GO and for functionalized GOs. The performance is better than that of other GO with no functionalization. The performance is worse than that of some functionalized GO or composites containing GO.

The effect of calcium on TC adsorption was explored in more detail by investigating the removal at eight different

Table 1 Comparison of the Adsorption Capacity of GO with other graphenic adsorbents for TC

Adsorbents	Experimental conditions	Q_{max} (mg g^{-1})	K_L (L mg^{-1})	Reference
GO	pH 4	104.30	0.08	[43]
GO-PLA	pH 4	223.70	0.15	
GO/Co–Fe	pH 7	60.24	140.80	[22]
GO-c-CD nano-composite	pH 8	322.58	0.02	[3]
A-mGO-Si	pH 7	59.01	0.31	[51]
GO	pH 5, no $CaCl_2$	185.60	0.05	*This study*
	pH 5, with $CaCl_2$	156.34	0.02	
	pH 9.5, with $CaCl_2$	113.75	0.05	

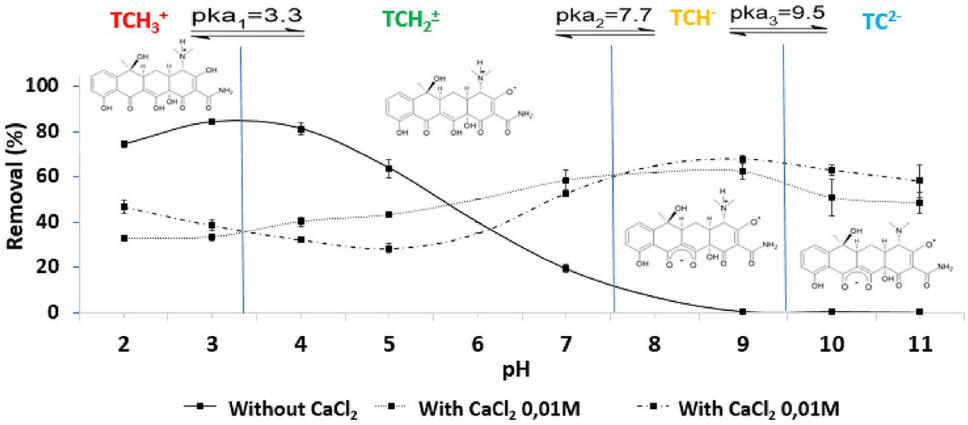

Fig. 6 Effect of pH in presence of Ca^{2+} on the adsorption of TC in GO. GO dose 250 mg L^{-1} and initial TC concentration of 30 mg L^{-1}

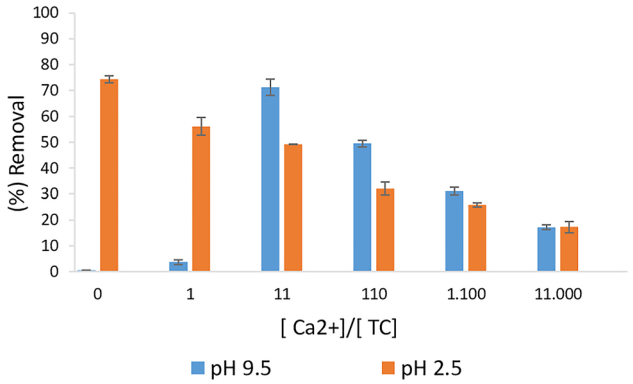

Fig. 7 Effect of $CaCl_2$ concentration on TC adsorption on GO at pH 9.5. GO dose 250 mg L^{-1} and initial concentration of TC 30 mg L^{-1}. Ca^{2+}/TC: ratio of molar concentrations

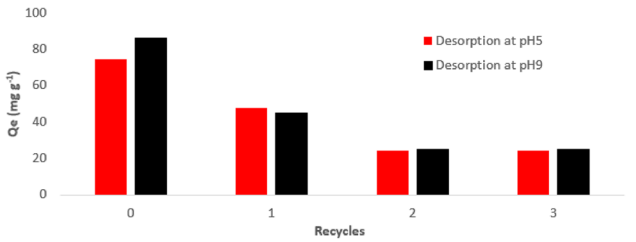

Fig. 8 Reusability of GO for TC adsorption. At pH 5 the adsorption step was conducted in pure water, since this is a situation where high adsorption is attained. At pH 9, the adsorption step was conducted in the presence of 0.01 M $CaCl_2$, for the same reason

pH values and at three different calcium concentrations. The results are shown in Fig. 6, and can be understood as an interplay between the two main roles played by calcium on TC adsorption, i.e., competitor or bridging cation. At pH lower than around 6, the competitor role of calcium prevails and thus TC removal decreased by increasing calcium concentration to 0.001 M or 0.01 M. At pH higher than around 6, on the contrary, calcium seems to act mainly as a bridge between the surface and TC, increasing TC removal by increasing calcium concentration to 0.001 M or 0.01 M. The general effect of calcium is, then, to flatten the adsorption vs pH curves, making the removal only weakly dependent on pH.

The effects of calcium were further investigated by working at two extreme pH values (2.5 and 9.5), with six different calcium concentrations. The results are shown in Fig. 7, which presents TC removal at different Ca^{2+}/TC ratios, for a constant TC concentration. At pH 2.5, where TC is fully in its cationic form, the results in Fig. 7 are typical of competition between calcium and TC for adsorption sites, with a monotonous decrease in TC adsorption as the Ca^{2+}/TC ratio increases. At pH 9.5, instead, the trend is no so simple. TC removal increases by increasing calcium concentration up to a Ca^{2+}/TC ratio of 11, passes through a maximum, and then decreases at higher Ca^{2+}/TC ratios. Bridging calcium may be still responsible for the adsorption under these conditions. However, it is very difficult to completely understand the whole behavior, especially why the removal decreased at very high calcium concentrations. At such high Ca^{2+} concentrations the surface probably becomes positively charged, as suggested by zeta potential data. In addition, the fact that the molar Ca^{2+} concentration is 11,000 times higher than that of TC may induce the formation of Ca^{2+}-TC species with an excess of calcium in the structure and low affinity for the surface. In fact, speciation calculations by Parolo et al. [45] showed that at high calcium concentrations and pH > 6 the dominant species in solution in a Ca^{2+}-TC mixture is Ca_2TC^{2+}, which may have low affinity for the positively charged GO surface.

Adsorption–desorption experiments using water at two different pH as eluent were conducted to check the reusability of GO for TC adsorption. As illustrated in Fig. 8, after three cycles of adsorption–desorption, there were similar decreases in the uptake performance for both pH used (32.68% at pH 5 and 29.56% at pH 9) that might be ascribed to partially irreversible adsorption that occupied some of the adsorption sites or the loss of adsorbent during the desorption process. Thus, due to the fact that the adsorbent

regeneration can be affected by various parameters such as the type and amount of the used reagent [14], the decrease in efficiency is acceptable, and further study on the use of a more efficient regeneration solution should be explored.

4 Conclusions

GO nanoparticles were prepared and characterized for TC adsorption. Adsorption varies widely with pH and Ca^{2+} concentration. In the absence of Ca^{2+}, adsorption was high at low pH and decreased as pH increased. It can be seen that in the presence of Ca^{2+} decreased TC adsorption at low pH but increased it at high pH. It is postulated that at least two different adsorption processes take place in the presence of Ca^{2+}: at $pH \leq 5$ there is cation exchange, and Ca^{2+} behaves as a competitor of the positively charged TC species. At $pH \geq 5$, the formation of Ca bridges (GO-Ca^{2+}-TC) is favored, increasing the adsorption of the antibiotic. Consequently, in the presence of Ca^{2+}, the pH does not produce significant variations in the adsorption of TC. The combination of Ca^{2+} and pH effects are important to optimize the behavior of GO and the use of Ca^{2+} or not will depend on the application needed. For example, not using calcium in the adsorbing media is important to reversibly adsorb TC at low pH and desorb it at high pH, which may be useful for decontamination and further regeneration of the adsorbent. Using Ca^{2+}, on the contrary, may be very advantageous for using GO in an electrochemical sensor, which will have a pH-independent response, facilitating the use of the device.

Supplementary Information The online version contains supplementary material available at https://doi.org/10.1007/s10450-024-00493-4.

Acknowledgements F.M Onaga Medina thanks CONICET for the research fellowship granted. Additionally, authors would like to thank Dr. Telma Musso (CIMAR PROBIEN, CONICET-Universidad Nacional del Comahue, Argentina) for XRD measurements.

Authors' contributions Florencia M. Onaga Medina: Conceptualization, Investigation, Writing—Original Draft, Methodology. Marcelo Javier Avena: Conceptualization, Supervision, Writing—Review & Editing. Maria E. Parolo: Conceptualization, Supervision, Writing—Review & Editing.

Funding Universidad Nacional del Comahue [grant number 04I252] and Universidad Nacional del Sur [grant number 24/Q120], (Argentina), and Foncyt for financial support.

Data availability All relevant data are included in this document or its supplementary material.

Declarations

Ethical Approval Not applicable.

Competing interests The authors declare that they have no conflict of interest.

References

1. Abdulghani, A.J., Jasim, H.H., Hassan, A.S.: Determination of tetracycline in pharmaceutical preparation by molecular and atomic absorption spectrophotometry and high performance liquid chromatography via complex formation with Au(III) and Hg(II) ions in solutions. Int. J. Anal. Chem. 2013(Il). (2013). https://doi.org/10.1155/2013/305124
2. Alazmi, A., Rasul, S., Patole, S.P., Costa, P.M.F.J.: Comparative study of synthesis and reduction methods for graphene oxide. Polyhedron **116**(April), 153–161 (2016). https://doi.org/10.1016/j.poly.2016.04.044
3. ALOthman, Z.A., AlMasoud, N., Mbianda, X.Y., Ali, I.: Synthesis and characterization of γ-cyclodextrin-graphene oxide nanocomposite: Sorption, kinetics, thermodynamics and simulation studies of tetracycline and chlortetracycline antibiotics removal in water. J. Mol. Liq. **345**(2022), 116993 (2022). https://doi.org/10.1016/j.molliq.2021.116993
4. Antelo, J., Arce, F., Fiol, S.: Arsenate and phosphate adsorption on ferrihydrite nanoparticles. Synergetic interaction with calcium ions. Chem. Geol. **410**, 53–62 (2015). https://doi.org/10.1016/j.chemgeo.2015.06.011
5. Bradder, P., Ling, S.K., Wang, S., Liu, S.: Dye adsorption on layered graphite oxide. J. Chem. Eng. Data **56**(1), 138–141 (2011). https://doi.org/10.1021/je101049g
6. Brigante, M., Parolo, M.E., Schulz, P.C., Avena, M.: Synthesis, characterization of mesoporous silica powders and application to antibiotic remotion from aqueous solution. Effect of supported Fe-oxide on the SiO2 adsorption properties. Powder Technol. **253**, 178–186 (2014). https://doi.org/10.1016/j.powtec.2013.11.008
7. Castellanos Lorduy, H.J., Pérez Cely, H.C., Casadiego Rincón, E.J., Henao Riveros, S.C., Colorado, C.L.: Cutibacterium Acnes Tetracycline Resistance Profile in Patients with Acne Vulgaris, in a Colombian Dermatologic Center. Actas Dermo-Sifiliograficas **112**(10), 873–880 (2021). https://doi.org/10.1016/j.ad.2021.05.004
8. Chen, D., Feng, H., Li, J.: Graphene oxide: Preparation, functionalization, and electrochemical applications. Chem. Rev. **112**(11), 6027–6053 (2012). https://doi.org/10.1021/cr300115g
9. Chen, X., Zhao, L., Tian, X., Lian, S., Huang, Z., Chen, X.: A novel electrochemiluminescence tetracyclines sensor based on a Ru(bpy)32+-doped silica nanoparticles/Nafion film modified electrode. Talanta **129**, 26–31 (2014). https://doi.org/10.1016/j.talanta.2014.04.054
10. Chopra, I., Roberts, M.: Tetracycline Antibiotics: Mode of Action, Applications, Molecular Biology, and Epidemiology of Bacterial Resistance. Microbiol. Mol. Biol. Rev. **65**(2), 232–260 (2001). https://doi.org/10.1128/mmbr.65.2.232-260.2001
11. Chowdhury, I., Mansukhani, N.D., Guiney, L.M., Hersam, M.C., Bouchard, D.: Aggregation and Stability of Reduced Graphene Oxide: Complex Roles of Divalent Cations, pH, and Natural Organic Matter. Environ. Sci. Technol. **49**(18), 10886–10893 (2015). https://doi.org/10.1021/acs.est.5b01866
12. Das, P., Mandal, B., Gumma, S.: Engineering of structural and surface functional characteristics of graphite oxide nanosheets by controlling oxidation temperature. App. Surf. Sci. 504(October 2019), 144444 (2020). https://doi.org/10.1016/j.apsusc.2019.144444
13. Dasenaki, M.E., Thomaidis, N.S.: Multi-residue determination of 115 veterinary drugs and pharmaceutical residues in milk powder, butter, fish tissue and eggs using liquid chromatography-tandem mass spectrometry. Anal. Chim. Acta **880**, 103–121 (2015). https://doi.org/10.1016/j.aca.2015.04.013
14. Ding, J., Pan, Y., Li, L., Liu, H., Zhang, Q., Gao, G., & Pan, B.: Synergetic adsorption and electrochemical classified recycling of Cr(VI) and dyes in synthetic dyeing wastewater. Chem. Eng. J. **384**(September 2019), 123232 (2020). https://doi.org/10.1016/j.cej.2019.123232
15. Drewniak, S., Muzyka, R., Stolarczyk, A., Pustelny, T., Kotyczka-Morańska, M., & Setkiewicz, M.: Studies of reduced graphene oxide and graphite oxide in the aspect of their possible application

in gas sensors. Sensors (Switzerland), 16(1). (2016). https://doi.org/10.3390/s16010103
16. Gao, W., Wu, G., Janicke, M.T., Cullen, D.A., Mukundan, R., Baldwin, J.K., Brosha, E.L., Galande, C., Ajayan, P.M., More, K.L., Dattelbaum, A.M., Zelenay, P.: Ozonated graphene oxide film as a proton-exchange membrane. Angewandte Chemie – Int. Edit. **53**(14), 3588–3593 (2014). https://doi.org/10.1002/anie.201310908
17. Gao, Y., Li, Y., Zhang, L., Huang, H., Hu, J., Shah, S.M., Su, X.: Adsorption and removal of tetracycline antibiotics from aqueous solution by graphene oxide. J. Colloid Interface Sci. **368**(1), 540–546 (2012). https://doi.org/10.1016/j.jcis.2011.11.015
18. Gao, Y.S., Xu, J.K., Lu, L.M., Wu, L.P., Zhang, K.X., Nie, T., Zhu, X.F., Wu, Y.: Overoxidized polypyrrole/graphene nanocomposite with good electrochemical performance as novel electrode material for the detection of adenine and guanine. Biosens. Bioelectron. **62**, 261–267 (2014). https://doi.org/10.1016/j.bios.2014.06.044
19. Guo, Z., Zhao, C., Yin, W., Xu, J., Zhang, Y., Shang, D., Wang, Q., Wang, J., Kong, Q.: Removal of tetracycline from water using activated carbon derived from the mixture of phragmites australis and waterworks sludge. ACS Omega **5**(26), 16045–16052 (2020). https://doi.org/10.1021/acsomega.0c01524
20. Han, Q.F., Zhao, S., Zhang, X.R., Wang, X.L., Song, C., Wang, S.G.: Distribution, combined pollution and risk assessment of antibiotics in typical marine aquaculture farms surrounding the Yellow Sea. North China. Environ. Int. **138**(January), 105551 (2020). https://doi.org/10.1016/j.envint.2020.105551
21. He, J., Fang, L.: Controllable synthesis of reduced graphene oxide. Curr. Appl. Phys. **16**(9), 1152–1158 (2016). https://doi.org/10.1016/j.cap.2016.06.011
22. Hossain, M.S., Kabir, M.H., Ali Shaikh, M.A., Haque, M.A., Yasmin, S.: Ultrafast and simultaneous removal of four tetracyclines from aqueous solutions using waste material-derived graphene oxide-supported cobalt-iron magnetic nanocomposites. RSC Adv. **14**(2), 1431–1444 (2024). https://doi.org/10.1039/d3ra07597d
23. Hou, Y., Lv, S., Liu, L., Liu, X.: High-quality preparation of graphene oxide via the Hummers' method: Understanding the roles of the intercalator, oxidant, and graphite particle size. Ceram. Int. **46**(2), 2392–2402 (2020). https://doi.org/10.1016/j.ceramint.2019.09.231
24. Ikonomidis, A., Venetis, C., Georgantzis, D., Giaslakiotis, V., Kolovos, V., Efstathiou, K., Moschou, M., Koutsiaris, E., & Panopoulou, M.: Prevalence of Chlamydia trachomatis, Ureaplasma spp., Mycoplasma genitalium and Mycoplasma hominis among outpatients in central Greece: Absence of tetracycline resistance gene tet(M) over a 4-year period study. New Microbes and New Infections, 9(M), 8–10. (2016). https://doi.org/10.1016/j.nmni.2015.11.005
25. Kartick, B., Srivastava, S.K., Srivastava, I.: Green synthesis of graphene. J. Nanosci. Nanotechnol. **13**(6), 4320–4324 (2013). https://doi.org/10.1166/jnn.2013.7461
26. Kumar, M., Jaiswal, S., Sodhi, K. K., Shree, P., Singh, D. K., Agrawal, P. K., Shukla, P.: Antibiotics bioremediation: Perspectives on its ecotoxicity and resistance. Environment International, 124(October 2018), 448–461. (2019). https://doi.org/10.1016/j.envint.2018.12.065
27. Li, C., Zhuang, Z., Jin, X., Chen, Z.: A facile and green preparation of reduced graphene oxide using Eucalyptus leaf extract. Appl. Surf. Sci. **422**, 469–474 (2017). https://doi.org/10.1016/j.apsusc.2017.06.032
28. Li, G., Shang, J., Wang, Y., Li, Y., Gao, H.: Effect of calcium on adsorption capacity of powdered activated carbon. J. Environ. Sci. (China) **25**(S1), S101–S105 (2013). https://doi.org/10.1016/S1001-0742(14)60636-7
29. Li, Y., Du, Q., Liu, T., Peng, X., Wang, J., Sun, J., Wang, Y., Wu, S., Wang, Z., Xia, Y., Xia, L.: Comparative study of methylene blue dye adsorption onto activated carbon, graphene oxide, and carbon nanotubes. Chem. Eng. Res. Des. **91**(2), 361–368 (2013). https://doi.org/10.1016/j.cherd.2012.07.007
30. Li, Y.H., Wang, S., Luan, Z., Ding, J., Xu, C., Wu, D.: Adsorption of cadmium(II) from aqueous solution by surface oxidized carbon nanotubes. Carbon **41**(5), 1057–1062 (2003). https://doi.org/10.1016/S0008-6223(02)00440-2
31. Lin, J., Jiang, B., Zhan, Y.: Effect of pre-treatment of bentonite with sodium and calcium ions on phosphate adsorption onto zirconium-modified bentonite. J. Environ. Manage. **217**, 183–195 (2018). https://doi.org/10.1016/j.jenvman.2018.03.079
32. Lin, J., Zhan, Y., Wang, H., Chu, M., Wang, C., He, Y., Wang, X.: Effect of calcium ion on phosphate adsorption onto hydrous zirconium oxide. Chem. Eng. J. **309**, 118–129 (2017). https://doi.org/10.1016/j.cej.2016.10.001
33. Liu, X., Huang, D., Lai, C., Zeng, G., Qin, L., Zhang, C., Yi, H., Li, B., Deng, R., Liu, S., Zhang, Y.: Recent advances in sensors for tetracycline antibiotics and their applications. TrAC - Trends Anal. Chem. **109**, 260–274 (2018). https://doi.org/10.1016/j.trac.2018.10.011
34. Lorenzetti, A.S., Sierra, T., Domini, C.E., Lista, A.G., Crevillen, A.G., Escarpa, A.: Electrochemically reduced graphene oxide-based screen-printed electrodes for total tetracycline determination by adsorptive transfer stripping differential pulse voltammetry. Sensors (Switzerland) **20**(1), 1–12 (2020). https://doi.org/10.3390/s20010076
35. Lu, L.M., Qiu, X.L., Zhang, X.B., Shen, G.L., Tan, W., Yu, R.Q.: Supramolecular assembly of enzyme on functionalized graphene for electrochemical biosensing. Biosens. Bioelectron. **45**(1), 102–107 (2013). https://doi.org/10.1016/j.bios.2013.01.065
36. Maged, A., Iqbal, J., Kharbish, S., Ismael, I.S., Bhatnagar, A.: Tuning tetracycline removal from aqueous solution onto activated 2:1 layered clay mineral: Characterization, sorption and mechanistic studies. J. Hazard. Mater. **384**, 121320 (2020). https://doi.org/10.1016/j.jhazmat.2019.121320
37. Marcano, D.C., Kosynkin, D.V., Berlin, J.M., Sinitskii, A., Sun, Z., Slesarev, A., Alemany, L.B., Lu, W., Tour, J.M.: Improved synthesis of graphene oxide. ACS Nano **4**(8), 4806–4814 (2010). https://doi.org/10.1021/nn1006368
38. Mendoza-Duarte, J.M., Robles-Hernández, F.C., Gomez-Esparza, C.D., Miranda-Hernández, J.G., Garay-Reyes, C.G., Estrada-Guel, I., Martínez-Sánchez, R.: Exfoliated graphite preparation based on an eco-friendly mechanochemical route. J. Environ. Chem. Eng. **8**(5), 104370 (2020). https://doi.org/10.1016/j.jece.2020.104370
39. Minale, M., Gu, Z., Guadie, A., Kabtamu, D.M., Li, Y., Wang, X.: Application of graphene-based materials for removal of tetracyclines using adsorption and photocatalytic-degradation: A review. J. Environ. Manage. **276**(June), 111310 (2020). https://doi.org/10.1016/j.jenvman.2020.111310
40. Mu, G., Liu, H., Xu, L., Tian, L., Luan, F.: Matrix Solid-Phase Dispersion Extraction and Capillary Electrophoresis Determination of Tetracycline Residues in Milk. Food Anal. Methods **5**(1), 148–153 (2012). https://doi.org/10.1007/s12161-011-9225-1
41. Mustapha, M., Goel, P., Mittal, D., Maan, S.: Molecular Investigations of Tetracycline Resistance Genes in Escherichia coli strains from Dogs Affected with Urinary Tract Infections. Alexandria J. Vet. Sci. **64**(1), 17 (2020). https://doi.org/10.5455/ajvs.64204
42. Ng, K., Linder, S.W.: HPLC separation of tetracycline analogues: Comparison study of laser-based polarimetric detection with UV detection. J. Chromatogr. Sci. **41**(9), 460–466 (2003). https://doi.org/10.1093/chromsci/41.9.460
43. Paleček, E., Bartošík, M.: Electrochemistry of nucleic acids. Chem. Rev. **112**(6), 3427–3481 (2012). https://doi.org/10.1021/cr200303p
44. Parolo, M.E., Savini, M.C., Vallés, J.M., Baschini, M.T., Avena, M.J.: Tetracycline adsorption on montmorillonite: pH and ionic strength effects. Appl. Clay Sci. **40**(1–4), 179–186 (2008). https://doi.org/10.1016/j.clay.2007.08.003
45. Parolo, M.E., Avena, M.J., Pettinari, G.R., Baschini, M.T.: Influence of Ca 2+ on tetracycline adsorption on montmorillonite. J. Colloid Interface Sci. **368**(1), 420–426 (2012). https://doi.org/10.1016/j.jcis.2011.10.079

46. Parolo, M.E., Avena, M.J., Savini, M.C., Baschini, M.T., Nicotra, V.: Adsorption and circular dichroism of tetracycline on sodium and calcium-montmorillonites. Colloids Surf., A **417**, 57–64 (2013). https://doi.org/10.1016/j.colsurfa.2012.10.060
47. Peng, L., Xu, Z., Liu, Z., Wei, Y., Sun, H., Li, Z., Zhao, X., Gao, C.: An iron-based green approach to 1-h production of single-layer graphene oxide. Nat. Commun. **6**, 1–9 (2015). https://doi.org/10.1038/ncomms6716
48. Pérez-Rodríguez, M., Pellerano, R. G., Pezza, L., & Pezza, H. R.: An overview of the main foodstuff sample preparation technologies for tetracycline residue determination. Talanta, 182(November 2017), 1–21. (2018). https://doi.org/10.1016/j.talanta.2018.01.058
49. Poh, H.L., Šaněk, F., Ambrosi, A., Zhao, G., Sofer, Z., Pumera, M.: Graphenes prepared by Staudenmaier, Hofmann and Hummers methods with consequent thermal exfoliation exhibit very different electrochemical properties. Nanoscale **4**(11), 3515–3522 (2012). https://doi.org/10.1039/c2nr30490b
50. Pradier, M., Robineau, O., Boucher, A., Titecat, M., Blondiaux, N., Valette, M., Loïez, C., Beltrand, E., Nguyen, S., Dézeque, H., Migaud, H., Senneville, E.: Suppressive antibiotic therapy with oral tetracyclines for prosthetic joint infections: a retrospective study of 78 patients. Infection **46**(1), 39–47 (2018). https://doi.org/10.1007/s15010-017-1077-1
51. Prarat, P., Hongsawat, P., Punyapalakul, P.: Amino-functionalized mesoporous silica-magnetic graphene oxide nanocomposites as water-dispersible adsorbents for the removal of the oxytetracycline antibiotic from aqueous solutions: adsorption performance, effects of coexisting ions, and natural organic. Environ. Sci. Pollut. Res. **27**(6), 6560–6576 (2020). https://doi.org/10.1007/s11356-019-07186-4
52. Rivera-Utrilla, J., Gómez-Pacheco, C.V., Sánchez-Polo, M., López-Peñalver, J.J., Ocampo-Pérez, R.: Tetracycline removal from water by adsorption/bioadsorption on activated carbons and sludge-derived adsorbents. J. Environ. Manage. **131**, 16–24 (2013). https://doi.org/10.1016/j.jenvman.2013.09.024
53. Romero, A., Lavin-Lopez, M.P., Sanchez-Silva, L., Valverde, J.L., Paton-Carrero, A.: Comparative study of different scalable routes to synthesize graphene oxide and reduced graphene oxide. Mater. Chem. Phys. **203**, 284–292 (2018). https://doi.org/10.1016/j.matchemphys.2017.10.013
54. Roy, S., Soin, N., Bajpai, R., Misra, D.S., McLaughlin, J.A., Roy, S.S.: Graphene oxide for electrochemical sensing applications. J. Mater. Chem. **21**(38), 14725–14731 (2011). https://doi.org/10.1039/c1jm12028j
55. Saleh, T. A., Sarı, A., & Tuzen, M.: Effective adsorption of antimony(III) from aqueous solutions by polyamide-graphene composite as a novel adsorbent. Chemical Engineering Journal, 307(Iii), 230–238. (2017). https://doi.org/10.1016/j.cej.2016.08.070
56. Sattayasamitsathit, S., Thavarungkul, P., Kanatharana, P.: Bismuth film electrode for analysis of tetracycline in flow injection system. Electroanalysis **19**(4), 502–505 (2007). https://doi.org/10.1002/elan.200603726
57. Song, X., Liu, H., Cheng, L., Qu, Y.: Surface modification of coconut-based activated carbon by liquid-phase oxidation and its effects on lead ion adsorption. Desalination **255**(1–3), 78–83 (2010). https://doi.org/10.1016/j.desal.2010.01.011
58. Srinivas, G., Burress, J.W., Ford, J., Yildirim, T.: Porous graphene oxide frameworks: Synthesis and gas sorption properties. J. Mater. Chem. **21**(30), 11323–11329 (2011). https://doi.org/10.1039/c1jm11699a
59. Stachowicz, M., Hiemstra, T., van Riemsdijk, W.H.: Multi-competitive interaction of As(III) and As(V) oxyanions with Ca2+, Mg2+, PO3-4, and CO2-3 ions on goethite. J. Colloid Interface Sci. **320**(2), 400–414 (2008). https://doi.org/10.1016/j.jcis.2008.01.007
60. Stobinski, L., Lesiak, B., Malolepszy, A., Mazurkiewicz, M., Mierzwa, B., Zemek, J., Jiricek, P., Bieloshapka, I.: Graphene oxide and reduced graphene oxide studied by the XRD, TEM and electron spectroscopy methods. J. Electron Spectrosc. Relat. Phenom. **195**, 145–154 (2014). https://doi.org/10.1016/j.elspec.2014.07.003
61. Sui, Z.Y., Cui, Y., Zhu, J.H., Han, B.H.: Preparation of Three-dimensional graphene oxide-polyethylenimine porous materials as dye and gas adsorbents. ACS Appl. Mater. Interfaces. **5**(18), 9172–9179 (2013). https://doi.org/10.1021/am402661t
62. Szabó, T., Szeri, A., Dékány, I.: Composite graphitic nanolayers prepared by self-assembly between finely dispersed graphite oxide and a cationic polymer. Carbon **43**(1), 87–94 (2005). https://doi.org/10.1016/j.carbon.2004.08.025
63. Topal, M., Arslan Topal, E.I.: Optimization of tetracycline removal with chitosan obtained from mussel shells using RSM. J. Ind. Eng. Chem. **84**(2019), 315–321 (2020). https://doi.org/10.1016/j.jiec.2020.01.013
64. Wang, C., Du, J., Wang, H., Zou, C., Jiang, F., Yang, P., Du, Y.: A facile electrochemical sensor based on reduced graphene oxide and Au nanoplates modified glassy carbon electrode for simultaneous detection of ascorbic acid, dopamine and uric acid. Sens. Actuators, B Chem. **204**, 302–309 (2014). https://doi.org/10.1016/j.snb.2014.07.077
65. Wang, H., Hu, Y.H.: Effect of oxygen content on structures of graphite oxides. Ind. Eng. Chem. Res. **50**(10), 6132–6137 (2011). https://doi.org/10.1021/ie102572q
66. Wong, A., Scontri, M., Materon, E.M., Lanza, M.R.V., Sotomayor, M.D.P.T.: Development and application of an electrochemical sensor modified with multi-walled carbon nanotubes and graphene oxide for the sensitive and selective detection of tetracycline. J. Electroanal. Chem. **757**, 250–257 (2015). https://doi.org/10.1016/j.jelechem.2015.10.001
67. Wong, A., Sotomayor, M.D.P.T.: Determination of carbofuran and diuron in FIA system using electrochemical sensor modified with organometallic complexes and graphene oxide. J. Electroanal. Chem. **731**, 163–171 (2014). https://doi.org/10.1016/j.jelechem.2014.08.025
68. Yao, T., Zhang, H., Feng, C., He, Y.: Continuous enrichment and trace analysis of tetracyclines in bovine milk using dual-functionalized aqueous biphasic system combined with high-performance liquid chromatography. J. Dairy Sci. **106**(9), 5916–5929 (2023). https://doi.org/10.3168/jds.2022-23034
69. Yu, C., Wang, C. F., Chen, S.: Facile Access to Graphene Oxide from Ferro-Induced Oxidation. Scientific Reports, 6. (2016) https://doi.org/10.1038/srep17071
70. Zhao, Q., Cheng, X., Wu, J., Yu, X.: Sulfur-free exfoliated graphite with large exfoliated volume: Preparation, characterization and its adsorption performance. J. Ind. Eng. Chem. **20**(6), 4028–4032 (2014). https://doi.org/10.1016/j.jiec.2014.01.002
71. Zhu, X., Lu, L., Duan, X., Zhang, K., Xu, J., Hu, D., Sun, H., Dong, L., Gao, Y., Wu, Y.: Efficient synthesis of graphene-multiwalled carbon nanotubes nanocomposite and its application in electrochemical sensing of diethylstilbestrol. J. Electroanal. Chem. **731**, 84–92 (2014). https://doi.org/10.1016/j.jelechem.2014.08.009